(Paper for the Special Issue on Computational Modeling of Concrete Materials)

Non-equilibrium thermodynamic modeling framework for OPC/SCM systems

Deborah Glosser, O. Burkan Isgor, and W. Jason Weiss

**Biography:** ACI member **Deborah** Glosser is a PhD candidate and ARCS scholar at Oregon State University. She received her MS in geophysics from the University of Pittsburgh. Her research interests include thermodynamic and multiphysics modeling of cement and metals-based materials.

FACI **O. Burkan Isgor** is a Professor in the School of Civil and Construction Engineering at Oregon State University. He is the chair of the ACI Committee 222 (Corrosion) and a member of ACI 365 and ACI 236. His research interests include corrosion of steel in concrete, service-life modeling, and non-destructive testing.

FACI **W. Jason Weiss** is the Edwards Distinguished Professor of Engineering and Head of the School of Civil and Construction Engineering at Oregon State University. His research interests include early age concrete, reducing the early age cracking potential of concrete, improving concrete durability, as well as service-life modeling.

#### **ABSTRACT**

Thermodynamic modeling is an established tool that can use binder composition to predict reaction products and pore solution chemistry in hydrating cementitious systems.

Thermodynamic simulations rely on the assumption that all reactions reach equilibrium;

however, reacting systems are inherently dynamic. An established kinetic model exists and is

used in conjunction with GEMS thermodynamic software to provide quasi-equilibrium inputs for modeling hydrating cement clinkers. However, no similar model has existed to explicitly model

the non-equilibrium reactions of cement with supplementary materials. Here, a framework to compute kinetic inputs for use in time-dependent thermodynamic calculations of cement/amorphous silica systems is demonstrated. Reaction products, pore solution composition, and pH are modeled and compared with experimental measurements for multiple OPC/SiO<sub>2</sub> binders at varying replacement levels and water contents. The results show that when time-dependent clinker and SiO<sub>2</sub> reactions are modeled together, the hydraulic reactions and the pozzolonicity of SiO<sub>2</sub> can be accurately predicted.

**Keywords:** ordinary portland cement; supplementary cementitious materials; thermodynamic modeling; dissolution kinetics; amorphous silica; hydration

#### INTRODUCTION

When modeling ordinary portland cement (OPC) systems, if the chemical composition of the constituent material is known, the hydrated phase assemblages and pore solution chemistry can be predicted as a function of time using thermodynamic modeling (1, 2). In such an approach, empirically-based kinetic equations can be used to describe the dissolution rates of the four main OPC clinker phases, which provide time-dependent input data for thermodynamic calculations. For example, the kinetic model developed by Parrot and Killoh (3) (henceforth the "PK" model") has been shown to reliably predict the dissolved amounts of C<sub>3</sub>A, C<sub>2</sub>S, C<sub>3</sub>S, and C<sub>4</sub>AF at different ages in most OPC-based systems (2-6). While other more complex models for simulating hydration kinetics exist (7, 8), and range from single particle models (9) to microstructural simulation models (10), the PK model is commonly used in conjunction with thermodynamic calculations because it provides a simple and accurate approach to predict reaction products based on starting information on the clinker composition (11-13). The combined PK/thermodynamic approach has proven to be a practical technique for predicting the evolution of OPC phase assemblages (14), porosity (6), and resistance to deleterious processes in aggressive environments (15) for specific mixtures, when experimental or empirical measurement is expensive or impractical.

Most modern binders however, are not made using only OPC, but incorporate supplementary cementitious materials (SCM) (16, 17). Thermodynamic modeling has also been used to predict the equilibrium products in cementitious systems containing SCM such as fly ash (18), slag (19), and silica fume (20). Historically, the modeling of OPC/SCM systems could only be accomplished for specific cement mixtures or conditions by two means: 1) by direct measurement of the SCM dissolution and fitting a rate equation to that specific system (20, 21);

or 2) by making simplifying assumptions about the dissolution and reaction rates of the SCM, such as assuming a constant reactivity over time (6). While the empirical fitting of a rate equation for each SCM is conceptually possible, it is rather restrictive in terms of using the data to predict reactions in unrelated systems. Therefore, a clear need exists for a simple dissolution kinetics model similar to the PK model that can be used specifically in conjunction with thermodynamic calculations to predict the composition of solid and liquid phases as a function of time, relative humidity, water-to-binder (w/b), binder composition, and temperature, in cementitious systems containing SCM.

Challenges involved in developing such models are due in part to SCM variability in composition (22), particle size and morphology (23), crystalline content (24), and ultimate reactivity (25), which can impact the hydraulic and pozzolanic reactions that can occur in OPC/SCM systems. In this paper, it is hypothesized that the PK equations may be modified to describe the reaction kinetics of SCM/OPC systems to be used in thermodynamic calculations, and we test this hypothesis using a simple system containing amorphous silica, with the main goal to provide a framework for thermodynamically modeling OPC-SCM systems. In a parallel work by the authors, this hypothesis was further tested and validated in a system containing OPC and fly ash (23).

Here, silica fume (SF) is used as a test case, as it is a simple and highly uniform (with low variability) pozzolanic SCM (26). The modified Parrot-Killoh model (MPK model) framework described in this paper extends the PK model to include this fifth phase, amorphous SiO<sub>2</sub>, in addition to the four clinker phases into the set of phase dissolution rates solved by equations. The MPK model, therefore, captures the combined dissolution kinetics of the four OPC clinker phases, as well as the amorphous SiO<sub>2</sub> phase. The inclusion of a fifth phase in the MPK model

will also have the effect of altering the dissolution rate each individual phase at any given time, in that replacing a portion of the clinker phases with amorphous SiO<sub>2</sub> will alter the overall system chemistry and the mass of clinker phase reacted at that time. The MPK model is then used to perform time-dependent thermodynamic calculations to predict the reactions of OPC/SiO<sub>2</sub> systems.

## RESEARCH SIGNIFICANCE

This work provides a new computational framework to drive the non-equilibrium thermodynamic modeling of cement/SCM mixtures. Thermodynamic modeling is a powerful tool for the prediction of pore solution chemistry, reaction products, and porosity in cementitious systems. Data from thermodynamic simulations are the link between a-priori information on bulk composition, and the prediction of properties in concrete, such as formation factor, freeze-thaw, and corrosion resistance. However, the time-dependent reaction processes that occur in reacting systems are inherently non-equilibrium. This paper demonstrates the proposed framework to calculate non-equilibrium inputs needed to thermodynamically model OPC/amorphous SiO<sub>2</sub> based on bulk composition.

#### **MODELING**

## **Background**

The original PK model describes the dissolution and hydration of the four principle clinker phases (C<sub>3</sub>S, C<sub>2</sub>S, C<sub>4</sub>AF, C<sub>3</sub>A) as a function of temperature, water-to-binder ratio (w/b), relative humidity, and powder specific surface area. The overall reaction rate is constrained by the slowest calculated rate of 1) nucleation and precipitation, 2) diffusion, and 3) hydrate shell growth for each phase (27). The PK model has been thoroughly validated for a range of OPC

mixtures (28). The empirical rate constants used in the PK model are calculated based on multiple measured dissolution and hydration rates of the four major clinker phases. In an OPC-based system, nucleation and growth tends to control early stages of hydration, followed by diffusion, and then at later stages, the slowing of transport (3). The specific dissolution rates and time that corresponds to the rate controlling equation will depend on the parameters of system being modeled. A benefit of the PK model is that while each rate equation is solved for each individual clinker phase at each time (giving a phase degree of hydration, DoH, at that time, which is based in part on the specific chemistry and mass of each clinker phase available for reaction), the overall system DoH at each time is also solved by the equations based on the weighted average of the individual phase DoH. In this regard, the PK approach models the combined reaction kinetics of the clinker phases, but not SCM.

# **Modeling Approach**

The MPK framework described in this paper is explicitly intended to be used in conjunction with thermodynamic calculations as a tool to predict dissolution rates, reaction products, and pore solution composition a function of time in OPC/amorphous silica systems. The MPK model incorporates the kinetics of four clinker phases and a fifth phase (amorphous SiO<sub>2</sub>). The amorphous SiO<sub>2</sub> is assumed to have a maximum degree of reactivity (DoR<sub>ph</sub>\*), which accounts for the availability of its components to participate in chemical reactions. For highly reactive material such as amorphous SiO<sub>2</sub>, this term may be assumed to be 100%, as done in this paper.

A benefit of the MPK approach over historic approaches that use thermodynamic calculations is that OPC and SCM reaction equations are coupled, and applicable to a broad range of OPC and amorphous SiO<sub>2</sub> binders and conditions. Historically, thermodynamic modeling of cement/SCM has required either simplifying assumptions on the dissolution of the SCM where all SCM phases

dissolve uniformly and linearly based on a measured or assumed maximum degree of reactivity (DoR\*) (29); or a kinetic model was fit to describe only the experimental system being modeled (21). The MPK model presents a framework for describing the kinetics of dissolution of any silica fume/cement system based on its bulk composition, using a parameterized function describing empirically observed behavior. This approach is intended to fill a need in the current computational work on thermodynamic modeling of modern cementitious binder by presenting a simple and easily modifiable framework for deriving the kinetic inputs needed for accurate thermodynamic modeling in silica fume/cement systems.

Conceptually, the difference between the MPK framework and a historical modeling approach of the use of the PK with assumed reactivity (PK + x% reactivity) (which ignores SCM kinetics) is shown in Figure 1. In the PK + x% reactivity approach, all of the SiO<sub>2</sub> is dissolved into solution at each time interval, while the cement phases dissolve over time. In the MPK approach, both the amorphous SiO<sub>2</sub> and cement phases have time dependencies. In other words, the dissolution rates change over time. It should be noted that the conceptual figure is a simplification for illustrative purposes, and is not intended to accurately depict rates or amounts of dissolution of any material. In Figure 1, x% reactivity is assumed to be 100%, although for other SCM it may be considerably lower for most SCM. However, since amorphous silica is generally considered to be highly reactive due to its 100% amorphous content and particle fineness, 100% reactivity is demonstrated here for conceptual simplicity.

# **MPK Model Equations**

The MPK model calculates the time dependent degrees of reaction,  $\alpha_{ph}(t)$ , of each phase (C<sub>3</sub>S, C<sub>2</sub>S, C<sub>3</sub>A, C<sub>4</sub>AF, and amorphous SiO<sub>2</sub>). The term "degree of reaction" as used here for simplicity

includes the pozzolanic reaction of the  $SiO_2$  and the hydraulic reactions of the clinker phases. The term is used in order to distinguish the time dependent reactions from the overall maximum degree of reactivity ( $DoR_{ph}^*$ ) of the amorphous silica (25).

$$\alpha_{ph}(t) = \int_0^t DoR_{ph}^* \left( \frac{A_{ph}}{A_0} min\{r_{ph,1}, r_{ph,2}, r_{ph,3}\} f_{w/b} \beta_H e^{\left(\frac{E_i}{R}\left(\frac{1}{T_0} - \frac{1}{T}\right)\right)} \right) dt$$
 1a

where  $DoR_{ph}^*$  is the maximum percent of SiO<sub>2</sub> available to react (which is assumed to be 100% in this work, but for SCM with lower reactivities, this term becomes smaller),  $A_{ph}$  (m<sup>2</sup>/kg) is the surface area of the clinker and SiO<sub>2</sub> phases, and  $A_o$  (m<sup>2</sup>/kg) is the reference surface area; T (K) is the modeling temperature,  $T_o$  (K) is the reference temperature (298.15 K);  $E_i$ , (J/mol) is the activation energy of each phase, R (8.314 J/mol-K) is the universal gas constant, and  $r_{ph,1}$ ,  $r_{ph,2}$  and  $r_{ph,2}$  are the rates of nucleation and precipitation, diffusion, and the slowing of transport of dissolved species, respectively, as follows:

$$r_{ph,1} = \frac{K_{ph,1}}{N_{ph,1}} \left( 1 - \alpha_{ph}(t) \right) \left( -\ln(1 - \alpha_{ph}(t)) \right)^{1 - N_{ph,1}}$$
 2a

$$r_{ph,2} = \frac{K_{ph,2}\sqrt[3]{(1-\alpha_{ph}(t))^2}}{1-\sqrt[3]{(1-\alpha_{ph}(t))}}$$
2b

$$r_{ph,3} = K_{ph,3(1-\alpha_{ph}(t))}^{N_{ph,3}}$$
 2c

The constants  $K_{ph,1}$ ,  $K_{ph,2}$ ,  $K_{ph,3}$  and  $N_{ph,1}$  and  $N_{ph,1}$  in Equations 2a-2c are empirical parameters which are used to calculate the reaction rate expressions of respective phases. These coefficients were fit from dissolution studies of OPC clinker phases and  $SiO_2$ . The original PK model contains  $K_{ph,1}$ ,  $K_{ph,2}$ ,  $K_{ph,3}$  and  $N_{ph,1}$  and  $N_{ph,3}$  parameters for four phases. The MPK model contains  $K_{ph,1}$ ,  $K_{ph,2}$ ,  $K_{ph,3}$  and  $N_{ph,1}$  and  $N_{ph,3}$  for five phases The numerical process used to

determine these coefficients for the MPK model are described in more detail in the following section of this paper.

The lowest value of  $r_{ph 1,2,3}$  at time t is considered the rate controlling step for dissolution for the respective phase at time t. The MPK model computes a degree of reaction  $\alpha_{ph}(t)$  for each of the five phases at that time, as well as an overall system degree of reaction, which is the weighted average of the degrees of reaction of each of the five phases. Note that in the original PK model, the overall degree of reaction is the weighted average of the degree of hydration of the four clinker phases. Including the fifth phase in the model means that the overall system degree of reaction is proportionally impacted by the replacement of the four OPC clinker phases by the fifth SiO<sub>2</sub> phase. Hence, the average system degree of reaction (and mass of each dissolved phase) at time t of a system using the original PK model will be different than that calculated using the MPK model. As a result, the acceleration or retardation of the reactions by the amorphous SiO<sub>2</sub> will be captured. Other oxides are allowed to dissolve in proportion to the overall system degree of hydration.

The factor that incorporates the influence of w/b in equation 1a,  $f_{w/b}$ , is given as:

$$f_{w/b} = (1 + 3.33 \times (H \times \frac{W}{b} - \alpha_t))^4 \text{ for } \alpha_t > H \times W/b$$

where H is a fitting factor added to the original PK model (14, 30)), which accounts for the reduction of the rate of reaction at later ages, particularly when w/b is low. The term  $\alpha_t$  refers to the average system degree of reaction at time t. The total system degree of hydration is taken as a weighted average for all phases. This is the same rationale employed in the original PK model and remains unchanged in the MPK model.

Finally, the effect of relative humidity on the degree of reaction is for the relative humidity  $(B_H)$ 

$$(B_H) = \left[ \frac{B_H - 0.55}{0.45} \right]^4 \tag{4}$$

In this work  $B_H$  is assumed to be 1 for saturated conditions, and remains unchanged from the original PK model. Future work may be completed to evaluate the effect of drying, and updates to this equation may be justified as a result.

# **Determination of fitting parameters for the MPK model**

To calculate the fitting parameters (K<sub>ph,1</sub>, K<sub>ph,2</sub>, K<sub>ph,3</sub>, N<sub>ph,1</sub>, N<sub>ph,3</sub>, and H) used to model dissolution rates for the MPK model, empirical measurements of the dissolution of amorphous SiO<sub>2</sub> over time were obtained from two experimental studies. These coefficients can be recalculated as additional experimental data become available. In the first study, Lothenbach et al. (26) measured dissolution in a 40% SiO<sub>2</sub> mass replacement (MR%) system with a w/b of 0.50. In the second study, Li et al. (31) measured dissolution in a 10% SiO<sub>2</sub> MR% system with a w/b of 1.0. The chemical composition of each is presented in Table 1. The SiO<sub>2</sub> used in Lothenbach et al. (26) study was a microsilica, and Li et al. (31) used a SiO<sub>2</sub> with a specific surface area of 21,400 m<sup>2</sup>/kg. Data from the studies included the mass of unreacted SiO<sub>2</sub> (g/100g) as determined by <sup>29</sup>Si MAS NMR at 8 different time intervals ranging from 0 to 1310 days; and from X-ray diffraction (XRD) and scanning electron microscopy (SEM) /energy dispersive X-ray analysis (EDX) at 5 different time intervals from 0 to 90 days, respectively, as shown in Tables 2 and 3.

Using the empirical SF dissolution data presented above, a nonlinear optimization method (Levenberg-Marquardt) (32) was used to calculate the fitting parameters (Table 4) for the MPK model. Constraints were set on the solution bounds to preclude negative solutions. The numerical optimization algorithm (solved using the Matlab computing environment) employed a least

squares technique to minimize the sum of the squares of the errors between the experimental data and the values calculated by the model. Using the parameters obtained from this analysis, the fit between the experimental data and the simulated data resulted in an R<sup>2</sup> value of 0.98 for the Lothenbach et al. (26) data and 0.97 for the Li et al. (31) data. Calculated coefficients were nearly identical using the data from both studies, with the exception of the K<sub>3</sub> and N<sub>3</sub> parameters. The differences in the computed K<sub>3</sub> and N<sub>3</sub> parameters are discussed later in the results section.

# Coupled thermodynamic/MPK modeling approach

The MPK model computes the degree of reaction of each phase at time *t*, which is converted to the mass (g) of each phase (i.e. C<sub>3</sub>S, C<sub>3</sub>S, C<sub>4</sub>AF, C<sub>3</sub>A, and SiO<sub>2</sub>) at time *t*. These numerical values are used in thermodynamic calculations to model the specific pozzolanic and hydration reactions and reaction products of these phases at each time, *t*. This enables a thermodynamic prediction of the type and amounts of solid reaction products, as well as the pore solution composition and pH.

Gibbs free energy minimization (GEMS) is used to perform thermodynamic calculations using the dissolved masses of each phase at time *t* that come from the MPK model (2, 17). GEMS3K is a geochemical modeling code that computes phase assemblage and speciation in geochemical and cementitious systems from bulk elemental compositions. GEMS requires information on the solubility of each phase. Thermodynamic data for cementitious materials were obtained from CemData v. 14.01 (33). The equilibrium speciation in the aqueous electrolyte solutions are calculated in GEMS (30). As a result, GEMS considers the solid, solid solution, and aqueous electrolytes simultaneously. The mass and type of dissolved species are predicted as well as type and amount of solid reaction products based on the stability of phases at system pH and

temperature. (2). Simulations were performed at a temperature of 25°C and at atmospheric pressure.

# COMPARISON OF MODEL TO EXPERIMENTAL AND THEORETICAL OBSERVATIONS

This section compares the MPK model framework using the fitted coefficients with experimental measurements. In addition, the results obtained from the MPK model are compared with those from another theoretical approach where equilibrium is assumed at all ages (as shown conceptually in Figure 1). First, the fitted MPK model coefficients that were obtained using the methods described in this paper are used to predict the dissolution rates of amorphous silica in other independent systems. Second, the MPK model results obtained using the two separate sets of empirical coefficients (Table 4e and 4f) are compared to one another. This was done to demonstrate that simply using the mean of the empirical coefficients (Table 4g) does not substantially impact the model results. Then, the MPK model's predictive ability for solid reaction products is validated against the results of several experimental studies measuring the calcium hydroxide (CH) concentration over time. The model results are also compared to a thermodynamic modeling approach, which does not incorporate time dependent kinetics, in order to demonstrate the benefit of the MPK approach over a common modeling approach. Finally, the MPK models' predictive ability to determine pore solution composition and pH is demonstrated by comparing the results of the model to several experimental studies, as well as against thermodynamic modeling without time dependent kinetics.

# Predicting amorphous SiO2 dissolution with the MPK model

The main goal of the MPK model is to provide the numerical input necessary for enable the kinetics of amorphous silica/cement systems to be modeled at non-equilibrium conditions. However before doing this it is used to first demonstrate that the model can accurately predict the dissolution rates of amorphous SiO<sub>2</sub> in other, independent systems. This is described in the following section.

To do so, dissolution data for silica fume as determined by  $^{29}$ Si MAS NMR were obtained from two published separate studies. In the first study by Muller et al. (34), silica fume dissolution was measured at 3, 7, 14, and 28 days. The w/b of the system studied by Muller et al. (34) was 0.40, and the silica fume was comprised of 98.6% amorphous SiO<sub>2</sub> with a specific surface area of 20 m<sup>2</sup>/g. The silica fume MR% was 10%. The average of the empirical coefficients (Table 4g) were used in the MPK model using the materials and test conditions in Muller et al. (34). The MPK model was able to accurately predict the dissolution of the amorphous silica ( $R^2 = 0.99$ ).

Data from a second separate independent study was used to further validate the MPK model's predictive ability for amorphous silica dissolution rates using silica fume dissolution data from another study by Lothenbach et al. (2012) (21) for a low alkali cement with a 10% mass replacement of silica fume comprised of 99.8% amorphous nanosilica and a w/b of 1.1. The MPK model was used with the average of the empirical coefficients (Table 4g). Table 6 shows the results of the model compared with the measured silica dissolution ( $r^2 = 0.99$ ).

# Choice of empirical coefficients for the MPK model

The Lothenbach et al. (26) and Li et al. (31) studies used to calibrate the model have different w/b ratios (0.5 and 1.0, respectively) and different SF MR% (40% and 10%, respectively). As

such, these results demonstrate that the average of the two sets of coefficients derived from these studies can accurately describe other systems. By using the average of the empirical parameters from these two studies in the model, a wide range of other SiO<sub>2</sub> /OPC systems can be accurately simulated. To this end, an SiO<sub>2</sub> /OPC system was modeled at a series of different amorphous silica MR% and w/b combinations at times ranging from 3-91 days. For each time step, MR% and w/b combination, the system was modeled twice: first, using the empirical coefficients derived from the experimental data of Lothenbach et al. (26), and second, using the empirical coefficients derived from the experimental data of Li et al. (31) In each case, the amounts of OPC clinker phases and SiO<sub>2</sub> at a given time were calculated using the MPK model, and these amounts were used as input for thermodynamic modeling to predict CH concentrations at various ages. Surface areas used in this study were 20,000 m<sup>2</sup>/kg for silica fume and 385 m<sup>2</sup>/kg for the clinker phases. The reference surface area of both the SF and clinker phases was 385 m<sup>2</sup>/kg, since a better fit was obtained when the SF surface area was taken as a ratio to the clinker surface area. The activation energy for SF was modeled as 80,000 J/mol, and the clinker phase activation energy was modeled as per Lothenbach et al. (14).

The predicted CH concentrations obtained for each time, MR%, and w/b combination from each model are compared to demonstrate internal consistency of the modeling approach. As seen in Table 4e and 4f, the numerical fitting procedure used to calculate the coefficients for SiO<sub>2</sub> dissolution rates from the Lothenbach et al. (26) and Li et al. (31) studies produced empirical values that are substantially similar to each other. This similarity suggests that the dissolution of amorphous siliceous material follows a predictable physical trend that can be described using numerical modeling. It is suggested that the average of each of the coefficients be used in future work. The CH content as calculated by the MPK model using the fitting parameters from the

Lothenbach et al. (26) and Li et al. (31) studies are shown in Figure 2, along with the experimentally measured values (discussed later) The clinker composition used in these test systems is shown in Table 5. The results obtained using the coefficients obtained from Lothenbach et al. (26) data are shown as black squares, and the results obtained from coefficients obtained from the Li et al. (31) data are shown as red polygons in Figure 2.

The first observation is that the concentration of CH predicted using the fitting parameters from Lothenbach et al. (26) versus Li et al. (31) data are nearly identical for each w/b, MR%, and time step, with the difference the two predictions typically falling within 1-2% of each other. It is expected that there is little difference between the two simulations, given the similarity in the empirical coefficients computed from both studies (Table 4). With the exception of the values for  $K_{SiO2,3}$  and  $N_{SiO2,3}$  the coefficients calculated from the Lothenbach et al. study are nearly identical to those calculated from the Li et al. (31) data (Table 4e and 4f). While these differences are not substantial, it is nevertheless instructive to consider when and why these differences may be influencing the model results.

The  $K_{ph,3}$  and  $N_{ph,3}$  coefficients are used in the calculation of the rate equation which describes the slowing of transport of dissolved species (Equation 2c). It is possible that the difference in  $K_{ph,3}$  and  $N_{ph,3}$  values fit from Lothenbach et al. (26) versus Li et al. (31) are a result of the higher MR% of SF used in the Lothenbach et al. (26) study (40%) than the Li et al. (31) study (10%). A 40% SF system would likely have a stronger filler effect than a 10% SF system, regardless of its chemical reactivity (20, 35). This would lead to an earlier slowing of dissolved species transport as pore occlusion from the dense packing of the SF between the proportionally larger cement grains results in the transport term becoming the rate limiting term at earlier time intervals. It is also possible that in a 10% MR case, the system would run out of SF earlier, resulting in a

difference in late age empirical result. In practice, it is likely (and demonstrated below) that the rate equation (1e) that uses these terms only applies at late stages of reaction and therefore is not implicated in the MPK predictions for early-mid stage reactions. Furthermore, when this rate equation is used by the MPK model, the overall difference in the calculated dissolution rate using either set of coefficients should be quite small. This is shown in Figure 2 and quantified in the following section.

To further illustrate both how the MPK model functions – as well as why the model produces nearly identical results using both sets of empirical coefficients – the MPK model was run using both sets of coefficients for an SiO<sub>2</sub> MR 10%, 0.50 w/b test system, and allowed to solve the three SiO<sub>2</sub> dissolution rate equations (2a – 2c) from 1 – 1000 days. Figure 3A and 3B shows the results of these simulations represented in g SiO<sub>2</sub>/g binder/day. Recall that the lowest rate (nucleation, diffusion, slowing of transport) is taken as the rate-controlling step. Hence, for each point in Figure 3 on the time axis, only the lowest corresponding value of either nucleation, diffusion, or slowing of transport on the rate axis is actually used to determine the absolute SiO<sub>2</sub> dissolution at that time. In practice, only the rate limiting step is used by the model in calculating the dissolution rate at each age.

In examining Figure 3A and B, several observations can be drawn: First, in both Figure 3A and 3B, each SiO<sub>2</sub> dissolution rate is nearly identical at each time comparing between simulations at early ages. Second, in both figures, the rate of nucleation (that corresponds to Equation 2a) is lowest in the first 10 days, the rate of diffusion (Equation 2b) is then lowest until roughly 70-80 days, and the rate of slowing of transport is lowest thereafter. The third observation is that as expected, the third rate equation using the K3 and N3 terms (Equation 2c) made from the coefficients obtained from Lothenbach et al. (26) data tend to be slightly smaller and apply

slightly earlier than those obtained from Li et al. (31) data. However, these differences are quite small and only apply at the latest stages of reaction, particularly after 500 days, when the former trends sharply downward (Figure 3A), whereas the later tends to plateau (Figure 3B) The fourth observation that can be made from Figure 2 is that the dissolution rates predicted by the model fall within the ranges predicted by experimental studies. For example, (26) (36) (21) report measured SiO<sub>2</sub> dissolution rates in of  $\sim 0.1$  g/g/day at 1 day,  $\sim 0.05$  g/g/day at 10 days, and 0.01 g/g/day at 100 days. The reported experimental results are substantially similar to those predicted by MPK using either set of empirical coefficients. These values also match the general qualitative understanding of SiO<sub>2</sub> reaction kinetics, in that the dissolution rate slows over time. These results demonstrate the accuracy of the MPK model, as well as support using the average value of the two sets of empirical coefficients in modeling. Finally, these results provide scientific insight as to the SiO<sub>2</sub> dissolution process. Specifically, the results provide information on the rate controlling process of SiO<sub>2</sub> dissolution at different ages. This information could be useful in building a comprehensive understanding of the reaction kinetics in siliceous systems, and well for the practical implementation of engineering practices aimed at optimizing mixtures based on underlying kinetics.

# Comparison between MPK model and experimental results for CH

The prior section demonstrated that the MPK model results are not significantly impacted by the choice of empirical coefficients. As a result, the average of each coefficient will be used for modeling. However, to validate the model itself, it is necessary to ensure that the model is able to reasonably match experimental results for separate test systems. Toward this end, thermodynamic calculations using GEMS were made using the input data generated from the MPK model to predict the CH concentrations of a series of different mixtures with various SF

MR% and w/b. The model predictions are compared to experimental measurements of CH at a series of different times.

Experiments were performed to obtain the CH content of a series of pastes as a function of time. The mixtures were composed of three SiO<sub>2</sub> MR% (2%, 5% and 8%), and two w/b (0.36 and 0.50). Pastes were prepared by adding the materials to a vacuum mixer for 90 seconds at 400 rpm. The mixer was stopped and sides were scraped to remove adhered material, and then further mixed for 90s at 400 rpm. Specimen curing was performed under ambient conditions (23°C) in cylindrical, sealed molds that were 38 mm by 50 mm in height. Samples were rotated continuously to minimize bleeding and segregation. Prior to testing, each sample was finely ground and passed through a 75-um sieve with a lathe grinder.

Thermogravimetric analysis (TGA) was performed at various ages (3, 7, 28, and 91 days) to quantify the amounts of CH present in the system. Approximately 30 mg of ground paste was placed in the TGA and heated to 1000°C at a rate of 10°C/minute in an inert nitrogen atmosphere. The CH amount was determined based on the mass loss between 380 and 460°C. A detailed description of methods used to determine CH amounts is described in (37) and (20). The SF used in this study contained 93.47% SiO<sub>2</sub> and had an LOI of 3.82. Other oxides were below the detection limit. The chemical composition of the clinker is given in Table 7.

Figure 2 shows the results of the experimental studies (black stars), plotted against the model results obtained using the coefficients obtained form the Lothenbach et al. (black squares) and Li et al. (red circles) data. As shown in Figure 2, and discussed in the prior section, the overall agreement between the CH amounts predicted by the MPK model (using fits from both the Lothenbach et al. (26) and Li et al. (31) studies) and the experiments for each test system is

strong. In general, the model results match the experiments within less <1 g/100g of paste, and are never off by more than 2.57 g/100g of paste.

The error is computed by subtracting the mass of CH measured for each experimental data point (i.e., each individual time, MR% and w/b) from the mass of CH predicted by the MPK model, and converted to a percent of the total binder. A total of 48 simulations were performed for this portion of the study (2 w/b × 3 MR% × 4 ages × 2 sets of empirical coefficients). Of the 48 simulations, 34 simulation results for CH concentration fall within <1 g/100g of paste of the experimental values. In other words, 71% of the simulation predictions have less than a 1% error from the experimental measurements. Only three simulation predictions are off from the experiments by more than 2 g/100g of paste. In other words, taken as a total percent of the volume of paste, the overall error between the model predictions and the experiments is typically less than 1%, and only >2% 0.06% of the time. These results provide supporting evidence that the modeling approach provides a framework that can be used to predict the dissolution rates and reaction kinetics of other OPC/SCM systems. Such an application of the framework has been demonstrated for OPC systems containing fly ash (23).

In addition to confirming that the model results predict the experimental results, another observation to draw from Figure 2 is that CH amounts decrease with increasing SF MR%. This is indicative of the greater pozzolonicity of materials made with a greater proportion of SF, both in terms of the rate of the reaction of the SiO<sub>2</sub> and the absolute amount reacted at each age. For example, the average modeled 91-day CH of the w/b 0.50 system is 9 grams versus 13 grams for a 8% and 2% SF MR%, respectively (Figure 2A and 2B). Similarly, the CH amounts tend to be lower in systems with a w/b of 0.36: For example, comparing Figure 2b and 1F, at a 2% SF MR%, the 91-day CH amount for the w/b 0.50 system is roughly 13 grams, versus 10 grams in

the w/b 0.36 case. These results not only match the measured experimental values, but also the range of values found in the literature (20, 38, 39).

# MPK framework versus historical PK + x% reactivity modeling approach

To demonstrate the contribution of the MPK model, it is important to understand how the MPK model compares to a model without kinetics. In this section, the MPK model is compared to an approach where the PK model is used for clinker kinetics, but time dependent SCM kinetics are ignored in the thermodynamic calculations, and the SCM (here, SiO<sub>2</sub>), is assumed to be 100% reactive and dissolve immediately. Since silica fume is predominantly amorphous silica, it is commonly assumed to be 100% reactive (40). This approach is referred to here as the "PK + 100% reactivity" approach (Figure 1). The main purpose of comparing the MPK model to the PK+100% reactivity approach is to demonstrate the importance of incorporating SCM kinetics into a thermodynamic model. Here, system CH concentrations at different time intervals are predicted using both the MPK model and the PK + 100% reactivity approach. Both model strategies are then compared to experimental measurements of CH concentrations at those ages. The purpose of these calculations is to emphasize the importance of accounting for the dissolution kinetics of the SCM phases when performing thermodynamic analysis in blended cementitious systems, and to demonstrate that ignoring SCM kinetics not only results in differences in the predicted amount of hydrates formed, but also in the reaction pathway. It should be noted that a 100% reactivity value is unrealistic for most SCM, since the amount of SCM that can react is a function of multiple factors, including glass content (24), particle size (41), particle morphology (42) and chemical composition (43). However, since amorphous silica is generally considered to be highly reactive due to its 100% amorphous content and particle fineness, 100% reactivity is demonstrated here for simplicity.

Figure 4 shows the experimental measurements of CH concentration for paste with a w/b 0.36 and 8% MR SiO<sub>2</sub> system (Table 5) measured at different time intervals (solid black stars), alongside the MPK model predictions (red circles), and the PK + 100% reactivity model (blue triangles). As seen in Figure 4, without a consideration of the kinetic effects, thermodynamic calculations can substantially overestimate the pozzolanicity of the SF, and seriously miscalculate the CH concentrations. The PK + 100% reactivity approach vastly underpredicts predicts CH content in the system. Using this approach, the CH content is predicted to be <1g/100 g of paste at every time except for 91 days, when it is predicted to be <2 g/100g. In reality, experimental measurements show that the CH content at is typically between 8 and 10 grams, and the MPK model predicts CH concentrations between roughly 8 and 9 grams. The PK + 100% reactivity calculations considerably underestimate the system CH content because the thermodynamic calculations assume that 100% of the SiO<sub>2</sub> dissolves immediately into solution using this approach: When this rapid influx of dissolved SiO<sub>2</sub> is used in the thermodynamic calculations, CH consumption that occurs in the pozzolanic reaction is predicted to be much greater than it actually is, resulting in very low predicted concentrations of CH. Furthermore, the rapid influx of dissolved SiO<sub>2</sub> alters the predicted pore solution pH, and therefore also the conditions for the formation and stability of hydrates predicted in PK + 100% reactivity calculations.

Similar comparisons of PK + 100% reactivity calculations which ignore SCM kinetics, and the MPK model are described in a later section with respect to the pore solution composition, and are described in that context.

# Comparison between MPK model and experimental results: pore solution

Pore solution pH

As shown in previous sections, the MPK modeling approach accurately predicts CH concentrations in multiple OPC/SiO<sub>2</sub> systems at various ages with low overall error as compared to the experiments. Since reactions in cementitious systems are mediated by the pore solution, it is also important to verify that the approach can accurately predict related factors such as pore solution pH, dissolved ion concentrations, and pore solution resistivity. To this end, pore solution pH composition and pore solution chemistry were obtained from Page and Vanesland (44) for OPC/SiO<sub>2</sub> mixtures of MR% 10, 20, and 30 and w/b of 0.50 and compared to MPK-based predictions. Chemical compositions of the materials are reported in the original paper (44), although it should also be noted that both the OPC and the SF used in the original study have relatively low alkali contents.

The pore solution pH at 10, 30, 60, and 84 days is shown in Figure 5 along with model comparisons. The quantity of alkali ions (mmol/100g) is shown in Figure 7, along with the model comparisons. For the MPK model, the average of the coefficients obtained from the Lothenbach et al. and Li et al. data were used (Table 4g).

There is a strong the relationship between the replacement of OPC by SiO<sub>2</sub>; reaction rates; and pore solution pH of these cementitious mixtures (45). Typically, OPC has a pore solution pH of roughly 13-13.5 (46). The addition of SiO<sub>2</sub> to cement has the effect of decreasing pore solution pH as a result of the dilution of OPC, as well as the uptake of alkalis from solution by calcium silicate hydrate (C-S-H) which is due to charge balance. This effect is magnified by having more C-S-H overall in a system that has been partially replaced by SiO<sub>2</sub>: When OPC is partially

replaced by SiO<sub>2</sub>, more CH is consumed in the pozzolanic reaction, and more C-S-H is formed as a result, which may increase the overall amount of alkali binding, leading to lower pore solution pH than in a plain OPC system. Additionally, the C-S-H that is formed has a lower calcium-silica ratio (C/S) than OPC, due to the higher proportion of silica in the mixture. Low C/S C-S-H uptakes more alkali than high C/S C-S-H (47).

Furthermore, the rate of SiO<sub>2</sub> dissolution both affects and is affected by the pH of the pore solution: When SiO<sub>2</sub> dissolves into solution, it causes a reduction in the solution pH as described above (38). However, it is a dynamic process: the reduction in the solution pH in turn slows the reaction of the SiO<sub>2</sub> (48). Over time, it would be expected that pore solution pH in highly siliceous systems should decline as most of the silica dissolves and reacts.

As shown in Figure 5, the MPK model and experimental measurements of pore solution pH capture expected trends in pore solution pH, and are nearly identical for all MR%. In all cases, the pore solution pH is highest at 10 days, and then decreases (or remains constant) between days 30 and 84. As described above, these trends and values are as expected for SiO<sub>2</sub>/OPC mixtures. The effect of MR% can be seen quite clearly in these results: The MR 10% system overall has the highest pore solution pH, followed by the MR 20% system, and then the MR 30% system. This reduction in pore solution pH as MR% increases is driven by the higher proportion of amorphous SiO<sub>2</sub> in the systems, and is not merely a dilution effect from reducing OPC. The close agreement between the experiments and model shows that the rate of the siliceous reactions is being accurately simulated using the MPK model and thermodynamic calculations.

Other pore solution properties

In addition to pore solution pH, the concentration of alkali ions (i.e.,  $Na^+$  and  $K^+$ ) in pore solution is also an important parameter to consider relative to the durability of cementitious mixtures. A decrease in alkali ion concentrations typically accompanies the decrease in pore solution pH. Furthermore, the concentration and activity of alkali ions influence pore solution resistivity and the susceptibility of a mixture to deleterious processes such as corrosion and ASR. For this reason, shown below are the experimental results for alkali concentrations and pore solution resistivity, as well as the predictions from the MPK model. The MPK model predictions and experimental results are further compared to the PK + 100% reactivity approach to demonstrate the need for the MPK model.

As with pH, the MPK model was compared to the experimental results from Page and Vennesland et al. (44) for alkali ion concentrations. The amount of available alkali ions in the pore solution at 84 days is shown in Figure 7 for MR 10%, MR 20%, and MR 30% as determined by both the MPK model and the laboratory measurements. The calculated ionic concentrations are also shown using the PK + 100% reactivity approach.

As with pore solution pH, the experimental results and MPK model results are in close agreement, typically within 3%. The trends observed in both cases are as expected. As the MR increases from 10% to 30%, the ionic concentrations for both Na<sup>+</sup> and K<sup>+</sup> decrease, and do so somewhat linearly with MR%. The error between the experiments and MPK model remains fairly consistent across MR%: Observing Figures 6A and 6B, the differences between the red circles (MPK model) and black stars (experiments) are ~1 mmol/100g for both K<sup>+</sup> (Figure 6A) and Na<sup>+</sup> (Figure 6B).

In observing the results of the PK + 100% reactivity model (blue triangles, in Figure 6), there is large error between the experimental measurements and the predictions. The concentrations of

both Na<sup>+</sup> and K<sup>+</sup> are substantially underpredicted by the PK + 100% reactivity model. The error between the experiments and the PK + 100% reactivity model also tends to increase with SF MR%, being the smallest at the MR 10% and greatest at MR 30% cases for both Na<sup>+</sup> and K<sup>+</sup>. The reason the MPK model more accurately predicts alkali ion concentrations relative to the PK + 100% reactivity model is likely due to the more accurate prediction of CH concentrations, and therefore C-S-H concentrations and alkali uptake. As shown in Figure 3, the PK + 100% reactivity kinetics vastly overpredicts CH consumption. It is likely that the model also overpredicts C-S-H production and alkali uptake within a similar magnitude, which results in lower alkali concentrations in the pore solution. Another potential factor for the superior prediction of alkali concentrations from the MPK model is the more accurate prediction of solubility and stability of solid hydration products that contain potassium and sodium: As shown, the MPK model accurately predicts pore solution pH, and therefore the thermodynamic calculations for the solid hydration products will more accurate, since stability and equilibrium formation of hydrates depends on pore solution pH.

# Pore solution resistivity

The concentration of alkali ions influences pore solution resistivity, which is an important consideration for the determination of formation factor, and the susceptibility of a system to corrosive processes. The pore solution resistivity at 84 days was simulated using PK + 100% reactivity calculations, and is compared to experimental measurements and to the MPK model predictions (Figure 7). As with the other pore solution results, the experimental measurements and MPK model predictions are in good agreement at all SiO<sub>2</sub> MR%. As expected, as SF MR% increases, the resistivity of the pore solution increases. The trend in model versus experimental agreement is similar to that observed in the Na+ and K+ concentrations (Figure 6), which is

unsurprising, given that these concentrations in the pore solution is a primary driver of pore solution resistivity along with OH-. In all cases, the MPK model better predicts pore solution resistivity than the PK + 100% reactivity model.

## **Conclusions**

This paper presents a computational approach (the MPK model) to incorporate the kinetic data needed for the non-equilibrium thermodynamic prediction of cement binders that contain amorphous SiO<sub>2</sub>. Specifically, this model enables the prediction of the individual phase dissolution rates of amorphous SiO<sub>2</sub> in addition to the four clinker phases, so that time-dependent thermodynamic calculations can be performed to determine pore solution pH and ionic concentration, resistivity, and reaction products in SiO<sub>2</sub>/OPC mixtures. The MPK model is explicitly designed as a simple framework to thermodynamically predict reaction products for any silica fume cement based on the initial binder composition. As such, it eliminates the need for the assumption of equilibrium or constant reactivity to be used to run GEMS models. Empirical coefficients for the siliceous components in the MPK model were calculated based on silica fume dissolution studies. The results of the model show that:

- 1. The MPK model produces more accurate inputs for thermodynamic calculations. This is an improvement over the historical approach that uses the Parrot Killoh + 100% SCM reactivity model (PK + 100% reactivity) and does not include SCM kinetics. As such, the MPK model can be used to more accurately predict both solid hydrated phase assemblages and pore solution composition.
- 2. The PK + 100% reactivity calculations underprecit CH concentrations at each age for OPC/amorphous SiO<sub>2</sub> systems, while the MPK model typically predicts CH

- concentration within 1% of experimental measurements. Similar magnitudes of accuracy are demonstrated for pore solution pH and alkali concentrations.
- 3. The MPK model predicts pore solution pH, ionic composition, and resistivity for multiple SF replacement levels and compositions, typically within 3% of experimental measurements.

This work fills an important gap in scaling GEMS to perform practical computations in that it presents a simple yet versatile modeling strategy that is capable of accurately capturing siliceous SCM kinetics in OPC/SiO<sub>2</sub> systems. The results of the model can be used to inform the prediction of important durability related properties of concrete systems, such as pH control for ASR, freeze-thaw resistance, and pore refinement for improving corrosion resistance. Importantly, the MPK modeling approach demonstrates that the PK model approach can be modified and applied to siliceous SCM systems.

# Acknowledgements

The authors gratefully acknowledge the financial support provided by ARPA-E, Energy Power Research Institute (EPRI), and National Science Foundation (Grant number NSF CMMI 1728358). The authors also acknowledge Dr. Prannoy Suraneni and Samantha Whatley for their laboratory assistance. Deborah would like to thank Dr. Russell Schwartz for his helpful consultation on nonlinear programming.

#### References

- 1. Lothenbach B, Winnefeld F, "Thermodynamic modelling of the hydration of portland cement," Cement and Concrete Research, V. 36, No. 2, Feb. 2006, pp. 209-26.
- 2. Jafari Azad V, Suraneni P, Isgor OB, Weiss WJ, "Interpreting the pore structure of hydrating cement phases through a synergistic use of the Powers-Brownyard model, hydration kinetics, and thermodynamic calculations," Advances in Civil Engineering Materials, V. 6, No. 1. 2017, pp. 201-38.
- 3. Parrot L, Killoh D, "Prediction of cement hydration," British Ceramic Proceedings, 1984, pp. 41-53.
- 4. Winnefeld F, Lothenbach B, "Hydration of calcium sulfoaluminate cements experimental findings and thermodynamic modelling," Cement and Concrete Research, V. 40, No. 8. 2010, pp. 1239-47.
- 5. Gruskovnjak A, Lothenbach B, Holzer L, Figi R, Winnefeld F, "Hydration of alkaliactivated slag: comparison with ordinary Portland cement," Advances in Cement Research, V. 18, No. 3, Jul. 2006, pp. 119-28.
- 6. Glosser D, Jafari Azad V, Suraneni P, Isgor B, Weiss WJ, "An extension of the Powers-Brownyard model to pastes Containing SCM," ACI Materials Journal, V. 116, No. 5. 2019, pp. 1-11.
- 7. Princigallo A, Lura P, van Breugel K, Levita G, "Early development of properties in a cement paste: A numerical and experimental study," Cement and Concrete Research, V. 33, No. 7, Jul. 2003, pp. 1013-20.
- 8. Voter AF, Montalenti F, Germann TC, "Extending the time-scale in atomistic simulations of materials," Annual Review of Materials Research, V. 32. 2002, pp. 321-46.

- 9. Kondo R, Kodama M, "On the hydration kinetics of cement," Semento Gijutsu Nenpo, V. 21. 1967, pp. 77-82.
- 10. Jennings HM, "A model for the microstructure of calcium silicate hydrate in cement paste," Cement and Concrete Research, V. 30, No. 1. 2000, pp. 101-16.
- 11. Suraneni P., Fu, T., Jafari-Azad, V., Isgor OB, Weiss WJ, "Pozzolanicity of finely ground lightweight aggregates,", Cement and Concrete Composites, V. 88, 2018, pp. 115-20.
- 12. Lothenbach B, Wieland E, "A thermodynamic approach to the hydration of sulphateresisting Portland cement," Waste Management, V. 26, No. 7. 2006, pp. 706-19.
- 13. Lothenbach B, Le Saout G, Gallucci E, Scrivener K, "Influence of limestone on the hydration of Portland cements," Cement and Concrete Research, V. 38, No. 6, Jun. 2008, pp. 848-60.
- 14. Lothenbach B, Matschei T, Moschner G, Glasser FP, "Thermodynamic modelling of the effect of temperature on the hydration and porosity of Portland cement," Cement and Concrete Research, V. 38, No. 1, Jan. 2008, pp. 1-18.
- 15. Jafari Azad V, Isgor OB, "Modeling chloride ingress in concrete with thermodynamically calculated chemical binding," International Journal of Advances in Engineering Sciences and Applied Mathematics, V. 9, No. 2. 2017, pp. 97-108.
- 16. Snellings R, Scrivener KL, "Rapid screening tests for supplementary cementitious materials: past and future," Materials and Structures, V. 49, No. 8, Aug. 2016, pp. 3265-79.
- 17. Lothenbach B, Scrivener K, Hooton RD, "Supplementary cementitious materials," Cement and Concrete Research, V. 41, No. 12. 2011, pp. 1244-56.

- 18. Rajabipour F, Giannini E, Dunant C, Ideker JH, Thomas MDA, "Alkali-silica reaction: Current understanding of the reaction mechanisms and the knowledge gaps," Cement and Concrete Research, V. 76, Oct. 2015, pp. 130-46.
- 19. Lothenbach B, Gruskovnjak A, "Hydration of alkali-activated slag: Thermodynamic modelling," Advances in Cement Research, V. 19, No. 2, Apr. 2007, pp. 81-92.
- 20. Whatley SN, Suraneni P, Azad VJ, Isgor OB, Weiss J, "Mitigation of calcium oxychloride formation in cement pastes using undensified silica fume," Journal of Materials in Civil Engineering, V. 29, No. 10, Oct. 2017.
- 21. Lothenbach B, La Saout G, Haha MB, "Hydration of a low-alkali CEM III/B–SiO2 cement (LAC)," Cement and Concrete Research, V. 42. 2012, pp. 412-23.
- 22. Angst U, Elsener B, Larsen CK, Vennesland O, "Critical chloride content in reinforced concrete A review," Cement and Concrete Research, V. 39, No. 12, Dec. 2009, pp. 1122-38.
- 23. Glosser D, Suraneni P, Isgor OB, Weiss WJ, "Estimating reaction kinetics of cementitious pastes containing fly ash," Cement and Concrete Composites, V. 112, Sept. 2020, 103655.
- 24. Durdzinski PT, Snellings R, Dunant CF, Ben Haha M, Scrivener KL, "Fly ash as an assemblage of model Ca-Mg-Na-aluminosilicate glasses," Cement and Concrete Research, V. 78, Dec. 2015, pp. 263-72.
- 25. Glosser D, Choudhary A, Isgor OB, Weiss WJ, "Special Issue Investigation of the reactivity of fly ash and its effect on mixture properties," ACI Materials Journal, V. 116, No. 4. 2019, pp. 193-200.
- 26. Lothenbach B, Rentsch D, Wieland E, "Hydration of a silica fume blended low-alkali shotcrete cement," Phys Chem Earth, V. 70, No. 71. 2014.

- Parrot L, Killoh D, "Prediction of cement hydration," British Ceramics Proceedings, V.
   1984, pp. 41-53.
- 28. Thomas JJ, Biernacki J, Bullard JW, "Modeling and simulation of cement hydration kinetics and microstructure development," Cement and Concrete Research, V. 41. 2011, pp. 1257-78.
- 29. Jafari Azad V, Isgor OB, "A thermodynamic perspective on admixed chloride limits of concrete produced with SCMs," Special Publication, V. 308. 2016, pp. 1-16.
- 30. Lothenbach B, Matschei T, Möschner G, Glasser FP, "Thermodynamic modelling of the effect of temperature on the hydration and porosity of Portland cement," Cement and Concrete Research, V. 38, No. 1. 2008, pp. 1-18.
- 31. Li S, Roy D, Kumar A, "Quantitative determination of pozzolons in hydrated systems of cement or calcium hydroxide with fly ash or silica fume," Cement and Concrete Research, V. 15. 1985, pp. 1079-86.
- 32. More J, Sorenson D, "The Levenberg-Marquardt Algorithm: Implementation and Theory," Book The Levenberg-Marquardt Algorithm: Implementation and Theory, Argonne National Labs, City, 1977.
- 33. Kulik D, Berner U, Curti E, "Modelling chemical equilibrium partitioning with the GEMS-PSI code." PSI Scientific Report, V. IV, Nuclear Energy and Safety, 2004.
- 34. Muller ACA, Scrivener K, Skibsted J, Gajewicz A, McDonald PJ, "Influence of silica fume on the microstructure of cement pastes: New insights from 1H NMR relaxometry," Cement and Concrete Research, V. 74. 2011, pp. 116-25.

- 35. De la Varga I, Castro J, Bentz D, Zunino F, Weiss W, "Evaluating the hydration of high volume fly ash mixtures using chemically inert fillers." Construction and Building Materials, V. 161. 2017, pp. 221-28.
- 36. Poulsen SL, Jakobsen HJ, "Methodologies for Measuring the Degree of Reaction of Portland Cement Blends with Supplementary Cement Materials by 29Si and 27Al MAS NMR Spectroscopy," Book Methodologies for Measuring the Degree of Reaction of Portland Cement Blends with Supplementary Cement Materials by 29Si and 27Al MAS NMR Spectroscopy 2009.
- 37. Kim T, Olek J, "Effects of sample preparation and interpretation of thermogravimetric curves on calcium hydroxide in hydrated pastes and mortars," Transportation Research Record Journal of the Transportation Research Board V. 2290. 2012, pp. 10-8.
- 38. Madani H, Bagheri A, Parhizkar T, "The pozzolanic reactivity of monodispersed nanosilica hydrosols and their influence on the hydration characteristics of Portland cement," Cement and Concrete Research, V. 42. 2012, pp. 1563-70.
- 39. Suraneni P, Weiss J, "Examining the pozzolanicity of supplementary cementitious materials using isothermal calorimetry and thermogravimetric analysis," Cement and Concrete Composites, V. 83. 2017, pp. 273-8.
- 40. Sun G, Brough A, Young F, "29Si NMR Study of the Hydration of Ca3SiO5 and b-Ca2SiO4 in the Presence of Silica Fum," J Am Ceram Soc, V. 82, No. 11. 1999, pp. 3225-30.
- 41. Costoya M, "Effect of Particle Size on the Hydration Kinetics and Microstructural Development of Tricalcium Silicate," Book Effect of Particle Size on the Hydration Kinetics and Microstructural Development of Tricalcium Silicate, Doctoral Thesis, Thesis No 4102, EPFL, 2008.

- 42. Suraneni P, Azad VJ, Isgor OB, Weiss WJ, "Use of fly ash to minimize deicing salt damage in concrete pavements," Transportation Research Record, No. 2629. 2017, pp. 24-32.
- 43. Suraneni P, Palacios M, Flatt RJ, "New insights into the hydration of slag in alkaline media using a micro-reactor approach," Cement and Concrete Research, V. 79, Jan. 2016, pp. 209-16.
- 44. Page CL, Vennesland Ø, "Pore solution composition and chloride binding capacity of silica-fume cement pastes," Matériaux et Construction, V. 16, No. 1, 1983/01/01. 1983, pp. 19-25.
- 45. Hong SY, Glasser FP, "Alkali binding in cement pastes Part I. The C-S-H phase," Cement and Concrete Research, V. 29, No. 12, Dec. 1999, pp. 1893-903.
- 46. Angst U, Elsener B, Larsen CK, Vennesland O, "Chloride induced reinforcement corrosion: Rate limiting step of early pitting corrosion," Electrochimica Acta, V. 56, No. 17, Jul 1. 2011, pp. 5877-89.
- 47. Zibara H, Hooton RD, Thomas MDA, Stanish K, "Influence of the C/S and C/A ratios of hydration products on the chloride ion binding capacity of lime-SF and lime-MK mixtures," Cement and Concrete Research, V. 38, No. 3, Mar. 2008, pp. 422-6.
- 48. Bickmore BR, Nagy A, "The effect of Al(OH)4- on the dissolution rate of quartz," Geochim Cosmochim Ac, V. 70. 2006, pp. 290-305.

#### LIST OF FIGURES

**Figure 1:** Conceptual figure showing the difference between the PK+ 100% reactivity model approach versus the MPK approach.

**Figure 2:** Results of CH (g/100 g binder) of simulations compared to experimental measurements.

**Figure 3:** SiO<sub>2</sub> dissolution rates (g/g/day) as calculated by the MPK model using the coefficients from A) Lothenbach et al. (26) and B) Li et al. (31).

**Figure 4:** Results of CH (g/100g) for w/b 0.36 MR% 10% system, experimentally determined (solid black stars) versus modeled with (red circles) and PK + 100% reactivity (blue triangles).

**Figure 5:** Pore solution pH measured by Page and Vennesland and Vanesland et al. (44) and as calculated by the MPK model.

**Figure 6:** A) K<sup>+</sup> (mmol/100g) and B) Na<sup>+</sup> (mmol/100g) measured at 84 days by Page and Vennesland and Vanesland (44) and as calculated using the MPK model, and thermodynamic calculations without SCM kinetics.

**Figure 7:** Pore solution resistivity calculated from data measured at 84 days by Page and Vennesland et al. (44) for MR 10%, MR 20%, and MR 30% and as calculated by the MPK model, and a thermodynamic model without SCM kinetics.

## LIST OF TABLES

- **Table 1:** Chemical composition of the SiO<sub>2</sub> from Lothenbach et al. (26) and Li et al. (31).
- **Table 2:** Reacted SiO<sub>2</sub> as determined by <sup>29</sup>Si MAS NMR from Lothenbach et al. (26).
- **Table 3:** Reacted SF as determined by selective dissolution from Li et al. (31).
- Table 4: Empirical fitting parameters calculated for SF (this study) and clinker phases (27).
- **Table 5:** Comparison of the MPK model predictions of dissolved amounts of silica fume with measured amounts in Muller et al. (34).
- **Table 6:** Comparison of the MPK model predictions of dissolved amounts of silica fume with measured amounts in Lothenbach et al. (2012) (21).
- **Table 7:** Chemical composition of the Type I/II OPC used in this study.

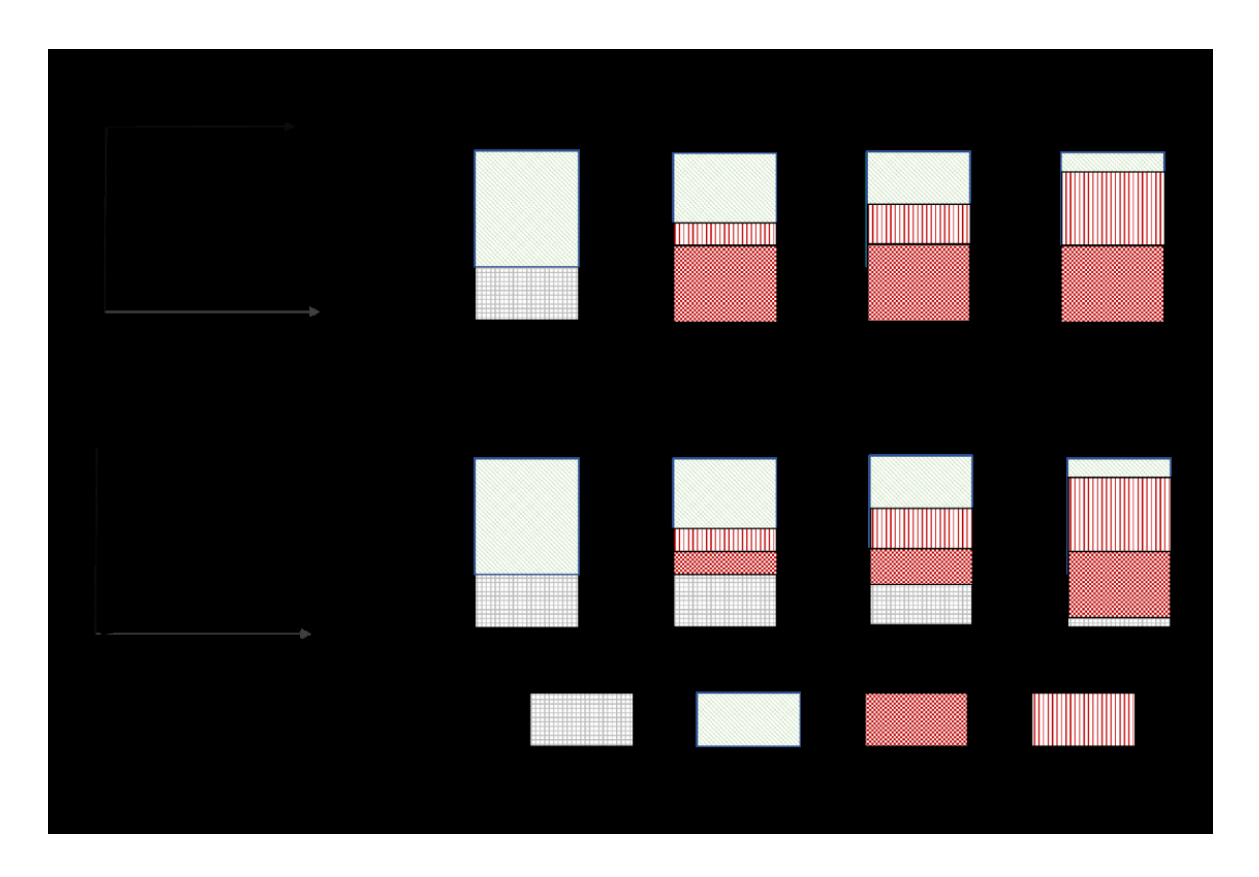


Figure 1: Conceptual figure showing the difference between the PK+ 100% reactivity model approach versus the MPK approach.

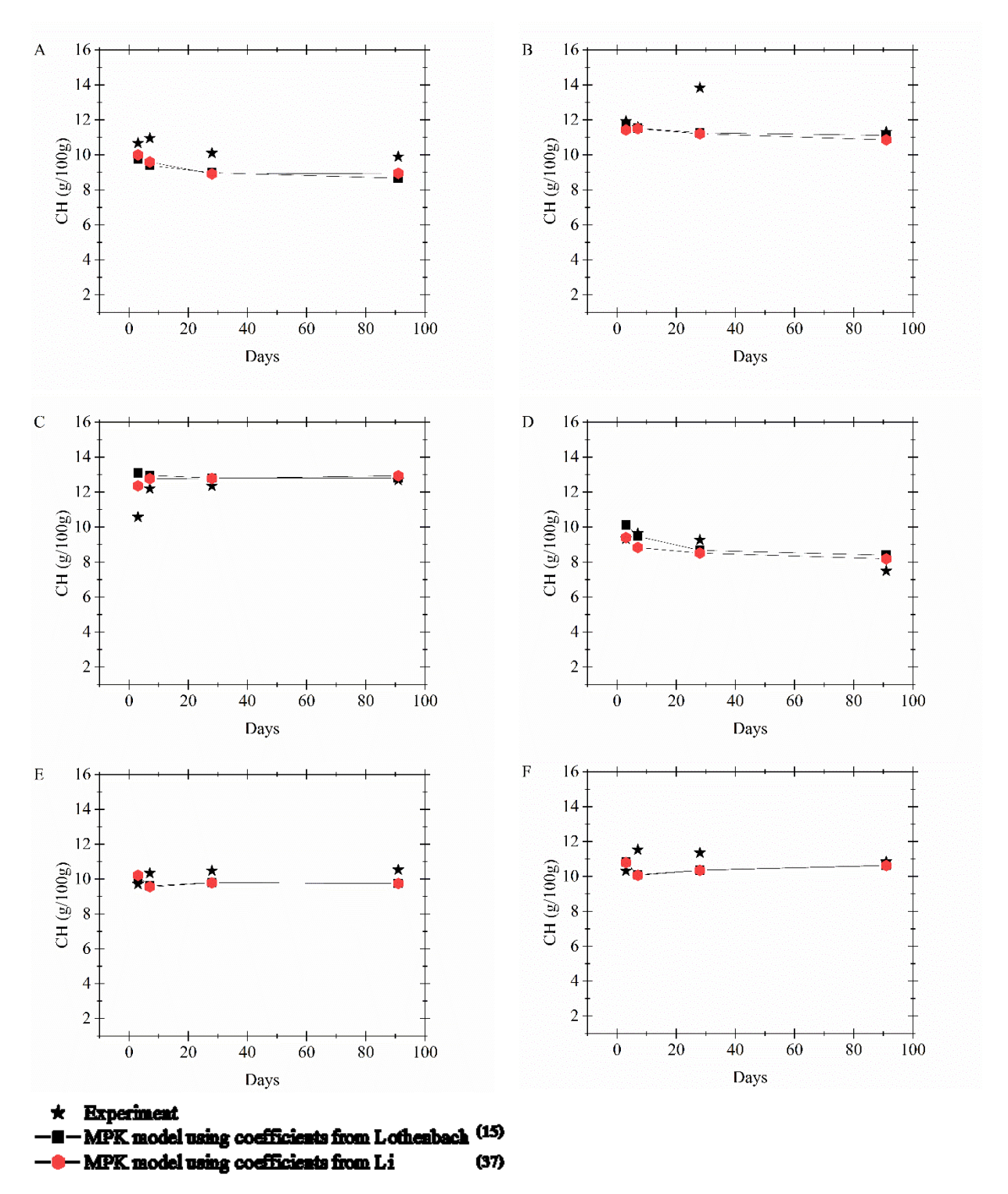


Figure 2: Results of CH (g/100 g binder) of simulations compared to experimental measurements. A) w/b 0.50, MR% 8%, B) w/b 0.50, MR% 5%, C) w/b 0.50 , MR% 2%, D) w/b 0.36 , MR% 8%, E) w/b 0.36 , MR% 5%, F) w/b 0.36 , MR% 2%.

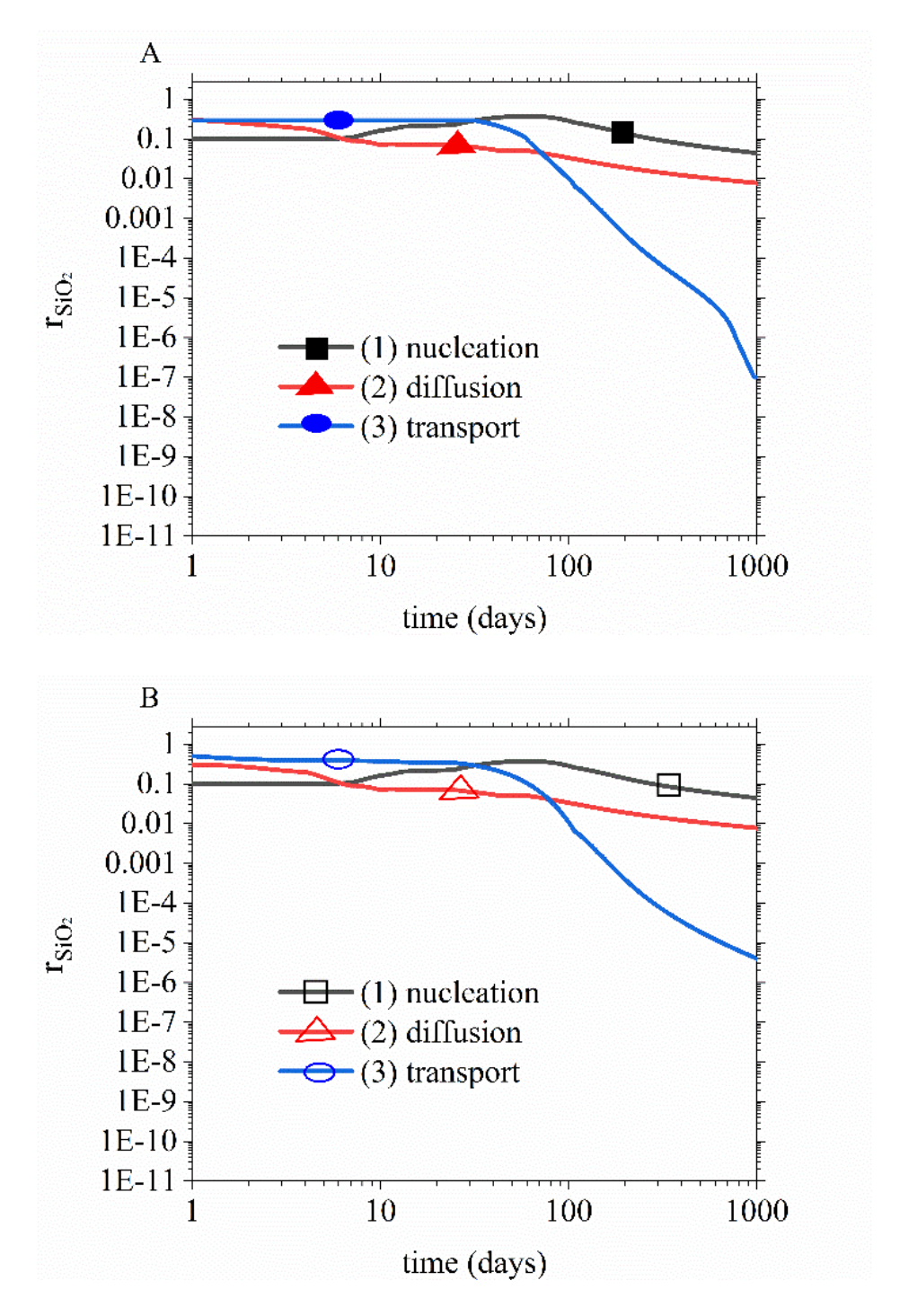


Figure 3: SiO<sub>2</sub> dissolution rates (g/g/day) as calculated by the MPK model using the coefficients from A) Lothenbach et al. (26) and B) Li et al. (31). Symbols added for clarity.

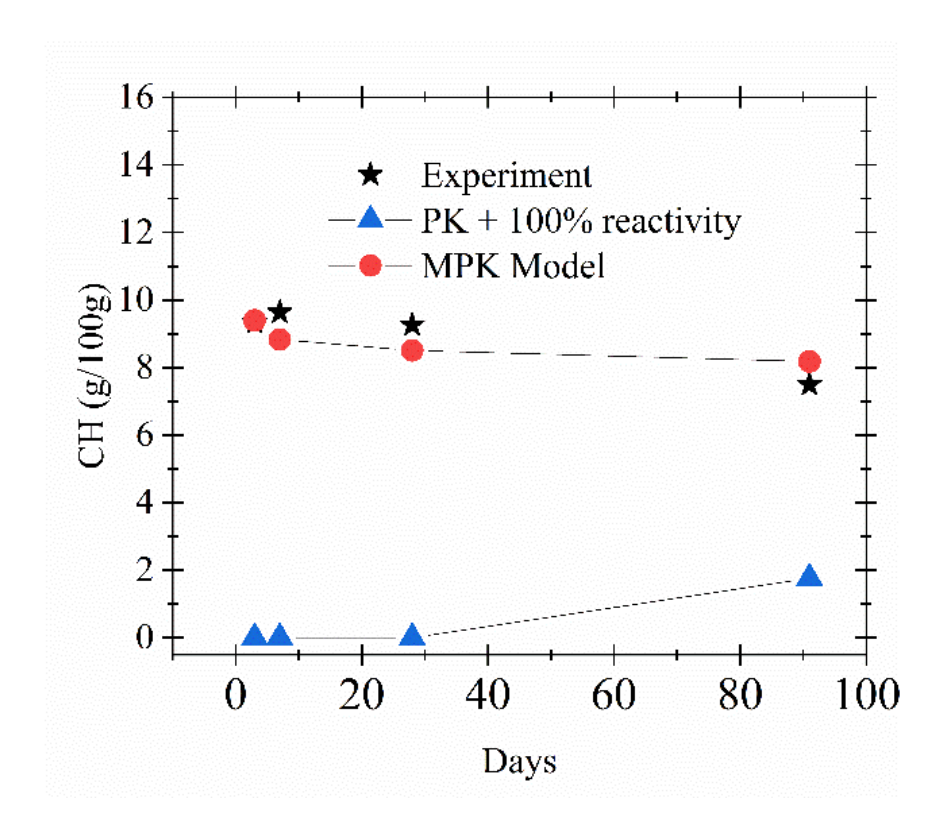


Figure 4: Results of CH (g/100g) for w/b 0.36 MR% 10% system, experimentally determined (solid black stars) versus modeled with (red circles) and PK + 100% reactivity (blue triangles).

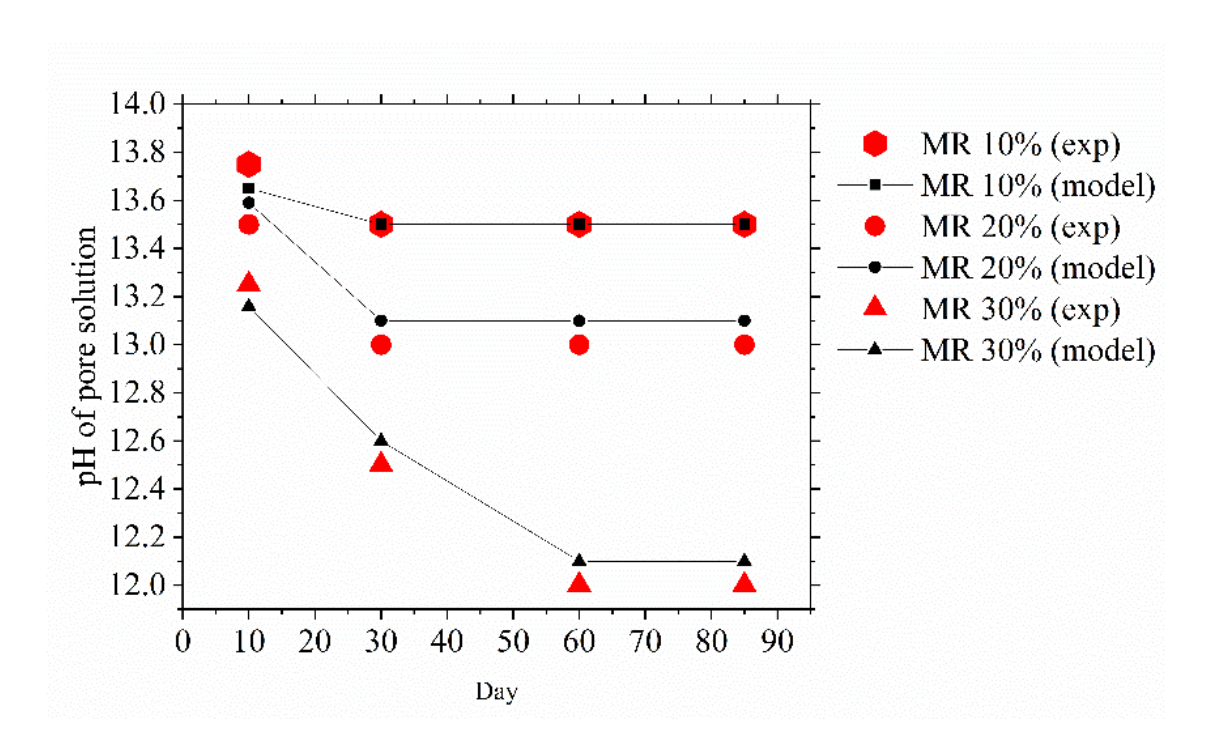


Figure 5: Pore solution pH measured by Page and Vennesland and Vanesland et al. (44) and as calculated by the MPK model.

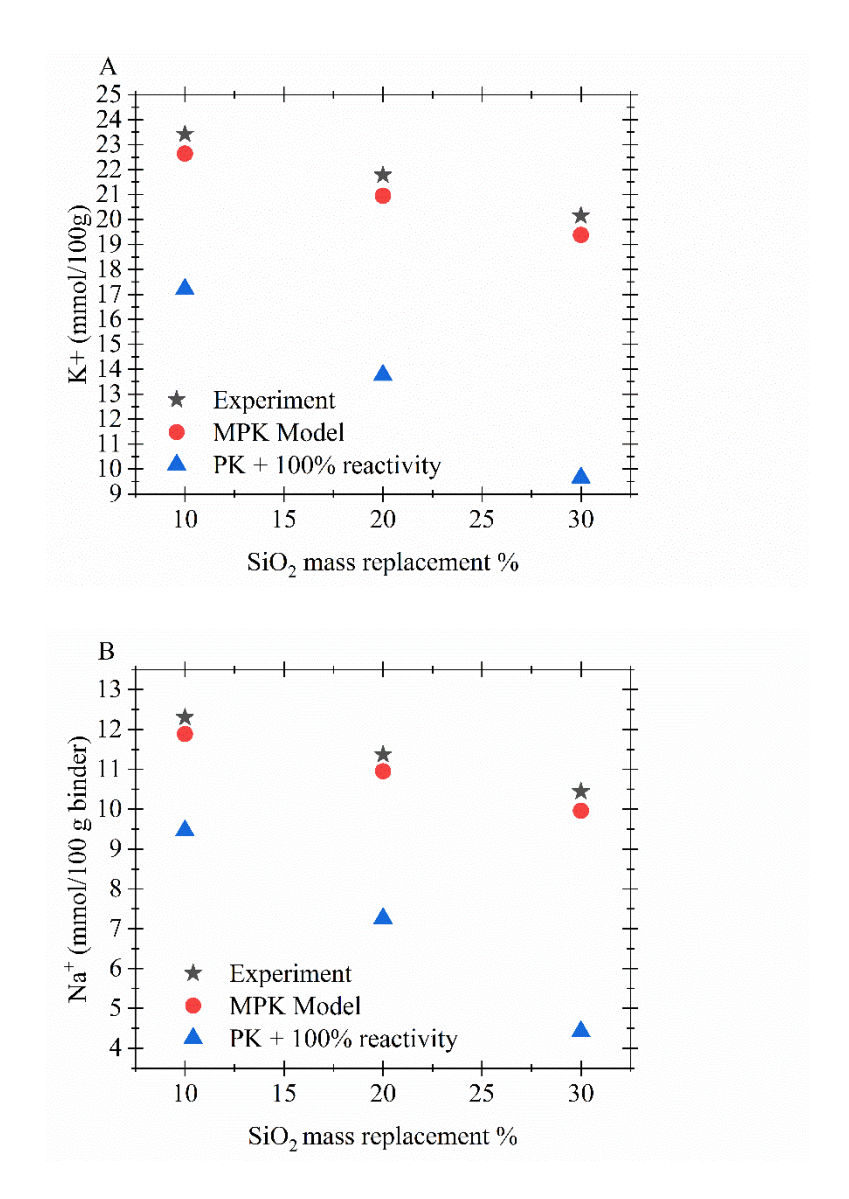


Figure 6: A) K<sup>+</sup> (mmol/100g) and B) Na<sup>+</sup> (mmol/100g) measured at 84 days by Page and Vennesland and Vanesland (44) and as calculated using the MPK model, and thermodynamic calculations without SCM kinetics.

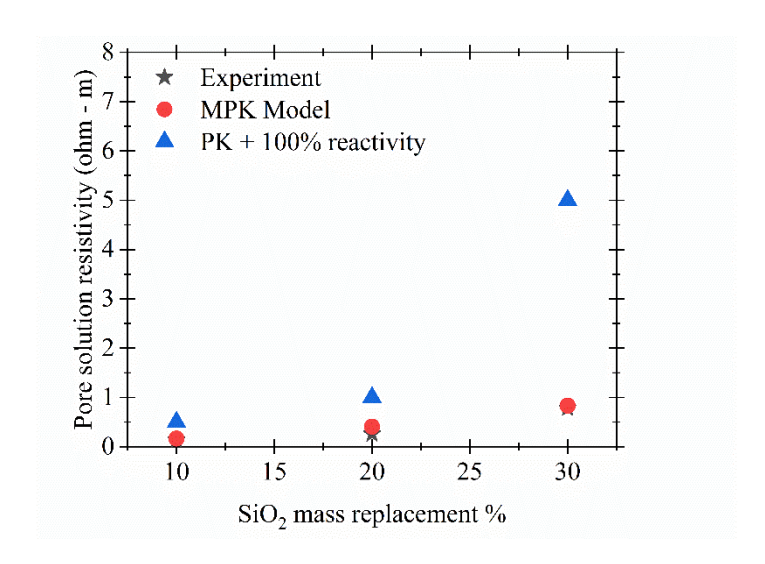


Figure 7: Pore solution resistivity calculated from data measured at 84 days by Page and Vennesland et al. (44) for MR 10%, MR 20%, and MR 30% and as calculated by the MPK model, and a thermodynamic model without SCM kinetics.

Table 1: Chemical composition of the SiO<sub>2</sub> from Lothenbach et al. (26) and Li et al. (31)

	Lothenbach et al. (26)	Li et al. (31)		
Oxide	Amount (%)	Amount (%)		
CaO	2.1	< 0.5		
SiO <sub>2</sub>	93.2	94.54		
Al <sub>2</sub> O <sub>3</sub>	0.19	0.10		
Fe <sub>2</sub> O <sub>3</sub>	0.13	0.20		
MgO	0.36	0.26		
Na <sub>2</sub> O	< 0.01	0.05		
K <sub>2</sub> O	0.51	0.45		
SO <sub>3</sub>	0.02	0.44		
Loss on ignition	3.10	3.57		
(LOI)				

Table 2: Reacted SiO<sub>2</sub> as determined by <sup>29</sup>Si MAS NMR from Lothenbach et al. (26)

Lothenbach et al. (26)					
Time (days)	Reacted SF (g/100g)				
0	0.00				
0.25	3.00				
4	9.00				
14	18.00				
28	23.00				
56	25.00				
356	28.00				
1310	30.00				

Table 3: Reacted SF as determined by selective dissolution from Li et al. (31)

<b>Li et al.</b> (31)				
Time (days)	Reacted SiO <sub>2</sub> (g/100g)			
0	0.00			
3	4.28			
7	5.68			
28	5.98			
90	7.08			

Table 4: Empirical fitting parameters calculated for SF (this study) and clinker phases (27)

	(a) C <sub>3</sub> S	(b) C <sub>2</sub> S	(c) C <sub>3</sub> A	(d) C4AF	(e) SiO <sub>2</sub> (26)	(f) SiO <sub>2</sub> (31)	(g) SiO <sub>2</sub> (avg)
K <sub>1</sub>	1.500	0.500	1.000	0.370	0.490	0.492	0.491
$N_1$	0.700	1.000	0.850	0.700	0.621	0.636	0.627
K <sub>2</sub>	0.050	0.006	0.040	0.015	0.050	0.043	0.047
K <sub>3</sub>	1.100	0.200	1.000	0.400	0.389	1.291	0.840
N <sub>3</sub>	3.300	5.000	3.200	3.70	3.426	3.142	3.284
Н	1.8	1.35	1.6	1.45	1.44	1.04	1.24

Table 5: Comparison of the MPK model predictions of dissolved amounts of silica fume with measured amounts in Muller et al. (34)

Day	Reacted SiO <sub>2</sub>	Reacted SiO <sub>2</sub>		
	g/100 g	g/100 g		
	(measured)	(MPK model)		
0	0	0		
3	3.4	3.2		
7	4	3.8		
14	6	5.9		
28	6.7	6.5		

Table 6: Comparison of the MPK model predictions of dissolved amounts of silica fume with measured amounts in Lothenbach et al. (2012) (21)

Day	g/100 g	g/100 g		
	(measured)	(MPK model)		
0	0.1	0		
1	2.5	2.3		
2	8.3	8		
7	9.1	8.5		
56	9.3	9		
1310	10	9.4		

Table 7: Chemical composition of the Type I/II OPC used in this study

C <sub>3</sub> S	C <sub>2</sub> S	C <sub>3</sub> A	C <sub>4</sub> AF	Na <sub>2</sub> O	K <sub>2</sub> O	MgO	SO <sub>3</sub>	LOI
59.53	12.35	6.84	10.14	0.30	0.28	0.81	3.12	2.92